PROCEEDINGS OF SCIENCE

Likelihood analysis of the general 2HDM with Gambit's FlavBit

Peter Athron,[a,b] **Csaba Balazs,**[b] **Tomás E. Gonzalo,**[c] **Douglas Jacob,**[b] **Farvah Mahmoudi**[d,e] **and Cristian Sierra**[b,*]

[a] *Department of Physics and Institute of Theoretical Physics, Nanjing Normal University, Wenyuan Road, Nanjing, Jiangsu, 210023, China*

[b] *School of Physics and Astronomy, Monash University, Wellington Road, Clayton, VIC 3800, Australia*

[c] *Institute for Theoretical Particle Physics and Cosmology (TTK), RWTH Aachen, Sommerfeldstrasse 12, 52074 Aachen, Germany*

[d] *Université de Lyon, Université Claude Bernard Lyon 1, CNRS/IN2P3, Institut de Physique des 2 Infinis de Lyon, UMR 5822, 69622 Villeurbanne, France*

[e] *Theoretical Physics Department, CERN, CH-1211 Geneva 23, Switzerland*

E-mail: cristian.sierra@monash.edu

We present a likelihood analysis of the general two Higgs doublet model, using the most important currently measured flavour observables, in view of the anomalies in charged current tree-level and neutral current one-loop rare decays of B mesons in $b \to c l \overline{\nu}$ and $b \to s\mu^+\mu^-$ transitions, respectively. Our analysis predicts values for $\mathrm{BR}(h \to \tau\mu)$ between 10^{-2} and 10^{-6} which are within the future sensitivity at the High Luminosity LHC. We also find that the predictions for the $\tau \to 3\mu$ and $\tau \to \mu\gamma$ decays are well within the projected limits of the Belle II experiment with a discovery potential for $\mathrm{BR}(\tau \to 3\mu) \sim 10^{-9}$ and $\mathrm{BR}(\tau \to \mu\gamma) \sim 10^{-9} - 10^{-8}$. Using the latest measurement of the Fermilab Muon $g-2$ Collaboration, we also perform a simultaneous fit to the muon anomalous magnetic moment and both observables related to flavour changing currents and leptonic decays of mesons, finding solutions at the 1σ level.

Computational Tools for High Energy Physics and Cosmology (CompTools2021)
22-26 November 2021
Institut de Physique des 2 Infinis (IP2I), Lyon, France

*Speaker

PoS(CompTools2021)011

1. Introduction

The two Higgs doublet model (2HDM) is one of the simplest ways to extend the Higgs sector, which is the least constrained sector of the Standard Model. Two Higgs doublets also appear in many more elaborate extensions of the SM that are based on fundamental principles, such as supersymmetry (see e.g. [1]), the Peccei-Quinn symmetry [2, 3] or grand unified theories (see [4] for a recent review).

The new interactions between the SM fermions and the physical states arising from the introduction of a second Higgs doublet imply a direct impact on lepton flavour universality (LFU) violation. Experimental measurements of LFU violation come from flavour changing charged currents (FCCCs), such as those in B meson decays, and flavour changing neutral currents (FCNCs), for instance in kaon decays. The observed deviations from the SM in the measurements of FCCCs (around 3.1σ from the SM [5]) and FCNCs (close to a combined 6σ deviation, see for example [6–8]), hint at the existence of new physics (NP) contributions and thus serve as a clear motivation for the study of NP models capable of explaining the anomalies.

It has indeed been shown that the general two Higgs doublet model (GTHDM) is able to explain the charged anomalies at 2σ [9–12]. Similar analyses for the neutral anomalies have also been presented previously [10, 13–15], finding solutions at the 2σ level and up to the 1σ level including right-handed neutrinos [15]. Nevertheless, the majority of these studies have only explored solutions in restricted regions of the parameter space, with a lack of discussion of the role of (marginally) statistically preferred regions, and often considering the $b \to sll$ observables from model independent global fits [10, 15]. On the other hand, statistically rigorous explorations of the parameter space have focused exclusively on interactions in the quark sector [16].

This conference paper presents some of the more important results obtained in [17] related to the flavour anomalies in the GTHDM, and is organised as follows. In section 2 we present the Yukawa sector of the GTHDM. In section 3 we define the effective Hamiltonian and the Wilson coefficients (WCs) for $b \to s\mu^+\mu^-$ transitions. Then, in section 4 we list the observables to be used in our scans. Following this, our results from the global fit and predictions for future experiments in colliders are discussed in section 5. Finally, we summarise our conclusions in section 6.

2. GTHDM

The GTHDM has been actively investigated in both its scalar and Yukawa sectors. These can be written in three different ways, namely in the generic, Higgs and physical bases, all of them related via basis transformations [18]. Here we review the Yukawa Lagrangian of the model as well as the relevant theoretical constraints coming from stability, unitarity and perturbativity at leading order (LO). We also make use of the precision electroweak constraints from the oblique parameters. For a more comprehensive review of the model the reader is referred to [19–22].

2.1 Yukawa Lagrangian

The most general Yukawa Lagrangian in the generic scalar basis $\{\Phi_1, \Phi_2\}$ reads [16]:

$$-\mathcal{L}_{Yukawa} = \bar{Q}^0 (Y_1^u \tilde{\Phi}_1 + Y_2^u \tilde{\Phi}_2) u_R^0 + \bar{Q}^0 (Y_1^d \Phi_1 + Y_2^d \Phi_2) d_R^0 + \bar{L}^0 (Y_1^l \Phi_1 + Y_2^l \Phi_2) l_R^0 + \text{h.c.}, \quad (1)$$

where the superscript "0" notation refers to the flavour eigenstates, and $\tilde{\Phi}_j = i\sigma_2\Phi_j^\dagger$. The fermion mass matrices are given by

$$M_f = \frac{1}{\sqrt{2}}(v_1 Y_1^f + v_2 Y_2^f), \qquad f = u, d, l. \tag{2}$$

Notice that this matrices need to be diagonalized. This can be done through a bi-unitary transformation

$$\bar{M}_f = V_{fL}^\dagger M_f V_{fR}, \tag{3}$$

where the fact that M_f is Hermitian implies that $V_{fL} = V_{fR}$, and the mass eigenstates for the fermions are given by

$$u = V_u^\dagger u^0, \qquad d = V_d^\dagger d^0, \qquad l = V_l^\dagger l^0. \tag{4}$$

Then, Eq. (2) takes the form

$$\bar{M}_f = \frac{1}{\sqrt{2}}(v_1 \tilde{Y}_1^f + v_2 \tilde{Y}_2^f), \tag{5}$$

where $\tilde{Y}_i^f = V_{fL}^\dagger Y_i^f V_{fR}$, though each Yukawa matrix is not diagonalized by this transformation. For this reason we shall drop the tilde from now on. Solving for Y_1^f we have

$$Y_{1,ba}^f = \frac{\sqrt{2}}{v\cos\beta}\bar{M}_{f,ba} - \tan\beta Y_{2,ba}^f. \tag{6}$$

Using the expressions above we can write the Yukawa Lagrangian in the mass basis as

$$\begin{aligned} -\mathcal{L}_{Yukawa} =& \bar{u}_b \left(V_{bc}\xi_{ca}^d P_R - V_{ca}\xi_{cb}^{u*} P_L\right) d_a H^+ + \bar{\nu}_b \xi_{ba}^l P_R l_a H^+ + \text{h.c.} \\ &+ \sum_{f=u,d,e} \sum_{\phi=h,H,A} \bar{f}_b \Gamma_{\phi ba}^f P_R f_a \phi + \text{h.c.}, \end{aligned} \tag{7}$$

where $a, b = 1, 2, 3$ and

$$\xi_{ba}^f \equiv \frac{Y_{2,ba}^f}{\cos\beta} - \frac{\sqrt{2}\tan\beta\bar{M}_{f,ba}}{v}, \tag{8}$$

$$\Gamma_{hba}^f \equiv \frac{\bar{M}_{f,ba}}{v} s_{\beta-\alpha} + \frac{1}{\sqrt{2}}\xi_{ba}^f c_{\beta-\alpha}, \tag{9}$$

$$\Gamma_{Hba}^f \equiv \frac{\bar{M}_{f,ba}}{v} c_{\beta-\alpha} - \frac{1}{\sqrt{2}}\xi_{ba}^f s_{\beta-\alpha}, \tag{10}$$

$$\Gamma_{Aba}^f \equiv \begin{cases} -\dfrac{i}{\sqrt{2}}\xi_{ba}^f & \text{if } f = u, \\ \dfrac{i}{\sqrt{2}}\xi_{ba}^f & \text{if } f = d, l. \end{cases} \tag{11}$$

At first, the total number of new complex Yukawa couplings to consider is 54. Considering only their real parts and the ansatz

$$\xi^u = \begin{pmatrix} 0 & 0 & 0 \\ 0 & \xi_{cc}^u & \xi_{ct}^u \\ 0 & \xi_{tc}^u & \xi_{tt}^u \end{pmatrix}, \qquad \xi^d = \begin{pmatrix} 0 & 0 & 0 \\ 0 & \xi_{ss}^d & \xi_{sb}^d \\ 0 & \xi_{bs}^d & \xi_{bb}^d \end{pmatrix}, \qquad \xi^l = \begin{pmatrix} 0 & 0 & 0 \\ 0 & \xi_{\mu\mu}^l & \xi_{\mu\tau}^l \\ 0 & \xi_{\tau\mu}^l & \xi_{\tau\tau}^l \end{pmatrix}, \tag{12}$$

we get only 12 Yukawa parameters (i.e., ignoring $3 \to 1$ and $2 \to 1$ generation transitions). Additionally, we will consider diagonal these matrices to be symmetric. Hence, the total number of parameters to scan over is reduced by 3.

3. Effective Hamiltonians for flavour changing transitions

There are only two independent flavour changing transitions that give rise to the majority of the studied observables, and these are the neutral $b \to s\ell^+\ell^-$ transition and the charged $b \to c\ell\bar{\nu}$ transition. In this section we write down the effective Hamiltonian for both of these transitions and provide expressions for the BSM contributions to the Wilson coefficients (WCs) that arise in our model.[1]

3.1 $b \to s\ell^+\ell^-$ transitions

The effective Hamiltonian responsible for $b \to s\ell^+\ell^-$ transitions can be written as

$$\mathcal{H}_{\text{eff}} = -\frac{4G_F}{\sqrt{2}} V_{tb}V_{ts}^* \left[\sum_{i=S,P} C_i(\mu)O_i + C_i'(\mu)O_i' + \sum_{i=7}^{10} C_i(\mu)O_i + C_i'(\mu)O_i' \right], \tag{13}$$

where μ is the energy scale at which the WCs are defined, and

$$O_9 = \frac{e^2}{16\pi^2}(\bar{s}\gamma_\mu P_L b)(\bar{\ell}\gamma^\mu \ell), \qquad O_{10} = \frac{e^2}{16\pi^2}(\bar{s}\gamma_\mu P_L b)(\bar{\ell}\gamma^\mu\gamma_5 \ell), \tag{14}$$

$$O_S = \frac{e^2}{16\pi^2} m_b(\bar{s}P_R b)(\bar{\ell}\ell), \qquad O_P = \frac{e^2}{16\pi^2} m_b(\bar{s}P_R b)(\bar{\ell}\gamma_5 \ell), \tag{15}$$

$$O_7 = \frac{e}{16\pi^2} m_b(\bar{s}\sigma^{\mu\nu}P_R b)F_{\mu\nu}, \qquad O_8 = \frac{g}{16\pi^2} m_b \bar{s}\sigma^{\mu\nu}T^a P_R b G^a_{\mu\nu}, \tag{16}$$

are the FCNC local operators encoding the low-energy description of the high energy physics that has been integrated out. The prime operators are obtained by the replacement $P_{R(L)} \to P_{L(R)}$. The WCs can be written as

$$C_i = C_i^{\text{SM}} + \Delta C_i, \tag{17}$$

where C_i^{SM} is the SM contribution to the ith WC and ΔC_i is the NP contribution, a prediction of the GTHDM model. The SM contribution to the scalar WCs, $C_{S,P}^{(\prime)}$, is negligible, whereas for C_{7-10} we have

$$\text{Re}(C_{7,8,9,10}^{\text{SM}}) = -0.297,\ -0.16,\ 4.22,\ -4.06, \tag{18}$$

as computed with SuperIso. We evaluate the NP scalar and pseudoscalar coefficients $\Delta C_{S,P}^{(\prime)}$ at tree level, which is the LO contribution from the GTHDM [15]. Henceforth we will use the scalar and pseudoscalar coefficients in the basis defined in SuperIso, i.e., $C_{Q_1,Q_2}^{(\prime)} = m_{b(s)} C_{S,P}^{(\prime)}$. The remaining coefficients, $\Delta C_{7,8,9,10}$ first appear at one loop level and we therefore include the one-loop BSM contributions to these in our analysis. These one-loop corrections can be split by contribution as follows,

$$\Delta C_{7,8} = C_{7,8}^{\gamma,g}, \tag{19}$$

$$\Delta C_9 = C_9^\gamma + C_9^Z + C_9^{\text{box}}, \tag{20}$$

$$\Delta C_{10} = C_{10}^Z + C_{10}^{\text{box}}. \tag{21}$$

[1] These BSM new contributions for $b \to s\ell^+\ell^-$ and $b \to c\ell\bar{\nu}$ transitions were included in our local version of FlavBit and might appear in a future release.

where $C^{Z}_{9,10}$ and $C^{\gamma}_{7,9}$ come from the Z and γ penguins, respectively (figure 1), and $C^{\text{box}}_{9,10}$ are contributions from box diagrams, (figure 2). C^{g}_{8} is the WC related to the chromomagnetic operator coming from gluon penguins and the NP contributions $\Delta C^{'}_{7,8}$ are computed in [15].

Using the model files provided by `FeynRules` from [23], we generate in `FeynArts` the one loop level Feynman diagrams for $b \to s\mu^+\mu^-$ transitions. After this, the amplitudes are tensor decomposed in`FeynCalc` [24] and then, the resulting Passarino-Veltman functions are Taylor expanded in the external momenta up to second order. Finally, the functions are integrated with `Package X` [25].[2]

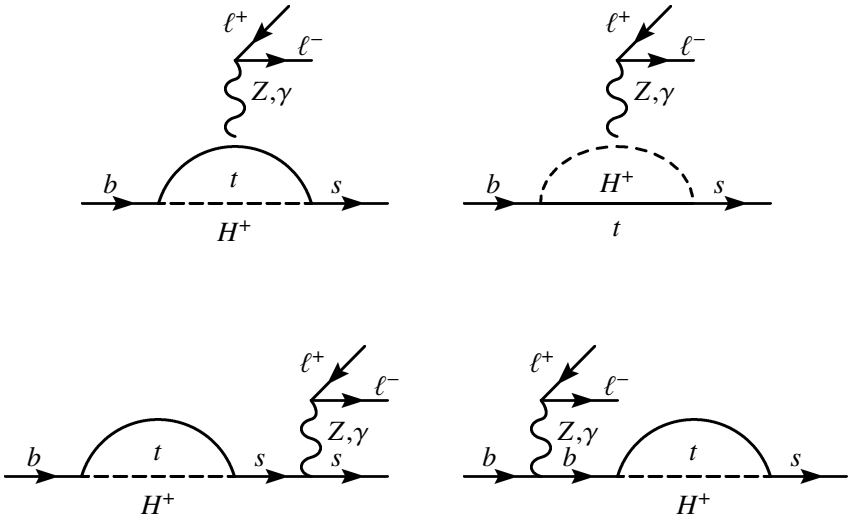

Figure 1: *Penguin diagrams for $b \to s\ell^+\ell^-$ transitions.*

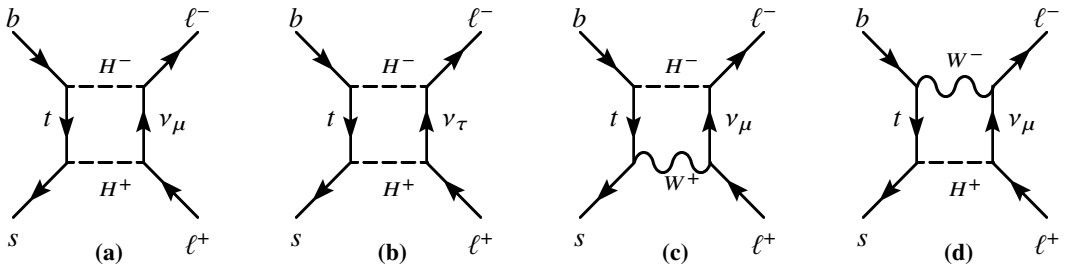

Figure 2: *Box diagrams for $b \to s\ell^+\ell^-$ transitions.*

3.2 $b \to c\ell\overline{\nu}$ semileptonic transitions

As a consequence of the new interactions between the fermions and the charged Higgs, semileptonic tree level flavour changing transitions appear in the GTHDM which have been extensively studied in the literature [10, 11, 22, 27–29]. Therefore we include tree-level calculations of the Wilson coefficients related to these in our analysis. The effective Hamiltonian responsible for the

[2]We additionally computed the WCs using the Modern ARtificial Theoretical phYsicist (`MARTY-1.4`) C++ package [26], obtaining a very good numerical agreement compared to the resultant expressions from `Package X`.

$b \to c\ell\overline{\nu}$ transitions for the semileptonic decays of B-mesons, including the SM and tree level GTHDM contributions can be written in terms of scalar operators in the form

$$\mathcal{H}_{\text{eff}} = C_{SM}^{cb} O_{SM}^{cb} + C_R^{cb} O_R^{cb} + C_L^{cb} O_L^{cb}, \tag{22}$$

where $C_{SM}^{cb} = 4G_F V_{cb}/\sqrt{2}$ and the operators are given by

$$\begin{aligned} O_{SM}^{cb} &= \left(\bar{c}\gamma_\mu P_L b\right)\left(\bar{\ell}\gamma_\mu P_L \nu\right), \\ O_R^{cb} &= \left(\bar{c} P_R b\right)\left(\bar{\ell} P_L \nu\right), \\ O_L^{cb} &= \left(\bar{c} P_L b\right)\left(\bar{\ell} P_L \nu\right). \end{aligned} \tag{23}$$

Given that the flavour of the neutrino in the final state can not be discerned by experiments, one has to add (incoherently) to the SM the NP contributions associated with the LFV couplings ξ_{ij}^l. The tree levelWCs C_R^{cb} and C_L^{cb} will be given by the expressions,

$$C_R^{cb} = -2\frac{(V_{cb}\xi_{bb}^d + V_{cs}\xi_{sb}^d)\xi_{\ell\ell'}^{l*}}{m_{H^\pm}^2}, \quad C_L^{cb} = 2\frac{V_{tb}\xi_{tc}^{u*}\xi_{\ell\ell'}^{l*}}{m_{H^\pm}^2}. \tag{24}$$

4. Observables

In this section we present the observables included in the fit. We divide them in four sets: The first one for FCNCs in $b \to s$ transitions and B meson rare decay observables, both of them affected by the new WC contributions. The second set is associated with FCCCs observables that arise from semileptonic $b \to c\ell\overline{\nu}$ decays and the mass difference ΔM_s from $B_s - \overline{B}_s$ oscillations. Various leptonic decays of mesons form the third set. Finally, the fourth set contains leptonic observables associated with τ and μ decays, among them the anomalous magnetic moment of the muon in particular.

4.1 FCNCs and B rare decays

The most interesting tests of LFU violation with FCNC are given by the ratios of $b \to sll$ transitions

$$R(K^{(*)}) = \frac{\Gamma(B \to K^{(*)}\mu^+\mu^-)}{\Gamma(B \to K^{(*)}e^+e^-)}, \tag{25}$$

with Γ representing the decay width and $K^{(*)}$ are kaons. As per our choice of Yukawa textures in Eq. (12), here we only consider NP effects coming from the muon specific WCs, i.e., electronic WCs are SM-like. Aside from this $R(K^{(*)})$ ratios, hints for LFU violation are found in many branching fractions and angular observables related to $B \to K^{(*)}\mu^+\mu^-$ decays as a function of the dimuon mass squared q^2. In this work we use the same observables as in [8], with the predicted values obtained with SuperIso and with likelihoods provided via HEPLike. A list of the included FCNC observables can be found in Table 1.

Observable	Experiment
$R(K^*)[0.045,\ 1.1]\ \text{GeV}^2$	$0.66 \pm 0.09 \pm 0.03$ [30]
$R(K^*)[1.1,\ 6.0]\ \text{GeV}^2$	$0.69 \pm 0.09 \pm 0.05$ [30]
$R(K)[1.1,\ 6.0]\ \text{GeV}^2$	$0.846 \pm 0.042 \pm 0.013$ [31]
$\text{BR}(B_s \to \mu^+\mu^-) \times 10^9$	$2.69^{+0.37}_{-0.35}$ [32]
$\text{BR}(B \to X_s\gamma) \times 10^4$	3.32 ± 0.15 [5]
$\text{BR}(B_s \to \tau^+\tau^-) \times 10^3$	< 6.8 at 95% C.L. [33]
$\text{BR}(B^+ \to K^+\tau^+\tau^-) \times 10^3$	< 2.25 at 90% C.L. [33]
$\text{BR}(B_s \to \mu^\pm\tau^\mp) \times 10^5$	< 4.2 at 95% C.L. [33]
$\text{BR}(B^+ \to K^+\mu^\pm\tau^\mp) \times 10^5$	< 4.8 at 90% C.L. [33]
$\mathcal{R}_K^{\nu\bar{\nu}}$	< 3.9 at 90% C.L. [34]
$\mathcal{R}_{K^*}^{\nu\bar{\nu}}$	< 2.7 at 90% C.L. [34]

Table 1: *Experimental measurements of FCNCs observables and bounds for rare B decays considered in our study. The $\mathcal{R}_{K^{(*)}}^{\nu\bar{\nu}}$ parameters are related to $b \to s\nu\bar{\nu}$ transitions as introduced in Eq.(4.6) in [15]. We also include all the angular distributions and branching fractions of $B^0 \to K^{*0}\mu^+\mu^-$ decays, the branching fractions of both $B_s \to \phi\mu^+\mu^-$ and $B^+ \to K^+\mu^+\mu^-$ with measurements provided by the HEPLikeData repository [35].*

4.2 FCCCs observables

The most relevant FCCC observables are the ratios of semileptonic B meson decays to τ and light leptons, that is

$$R(D^{(*)}) = \frac{\Gamma(\overline{B} \to D^{(*)}\tau\overline{\nu})}{\Gamma(\overline{B} \to D^{(*)}l\overline{\nu})}, \tag{26}$$

where $D^{(*)}$ are charmed mesons and l is either an electron (e) or a muon (μ). As of the time of writing, the world average for the experimental measurement of the ratios $R(D^{(*)})$ sits at a 3.1σ deviation from the SM prediction [5].

The GTHDM contributions to $R(D)$ and $R(D^*)$ from the effective Hamiltonian in Eq. (22) can be written as,

$$R(D) = \frac{1 + 1.5\,\text{Re}(g_S^{\tau\tau}) + 1.0\sum\left|g_S^{\tau l}\right|^2}{3.34 + 4.8\sum\left|g_S^{\mu l}\right|^2}, \tag{27}$$

$$R(D^*) = \frac{1 + 0.12\,\text{Re}(g_P^{\tau\tau}) + 0.05\sum\left|g_P^{\tau l}\right|^2}{3.89 + 0.25\sum\left|g_P^{\mu l}\right|^2}. \tag{28}$$

A summary of all FCCC observables included in this study is provided in Table 2.

Observable	Experiment
$R(D)$	$0.340 \pm 0.027 \pm 0.013$ [5]
$R(D^*)$	$0.295 \pm 0.011 \pm 0.008$ [5]
$R_{e/\mu}$	$1.01 \pm 0.01 \pm 0.03$ [36]
τ_{B_c}(ps)	0.510 ± 0.009 [33]
$F_L(D^*)$	$0.6 \pm 0.08 \pm 0.04$ [37]
$\Delta M_s(\text{ps}^{-1})$	17.741 ± 0.020 [5]

Table 2: *Observables related to the charged anomalies considered in our study. We also include the normalised distributions $d\Gamma(B \to D\tau\overline{\nu})/(\Gamma dq^2)$ and $d\Gamma(B \to D^\star\tau\overline{\nu})/(\Gamma dq^2)$ as measured by the BaBar collaboration [38].*

4.3 Leptonic decays of mesons

Beyond those described in Sections 4.1 and 4.2, there are additional leptonic decays included in this study. The total decay width at LO for the process $M \to l\nu$ in the GTHDM is computed as [21, 39, 40]

$$\text{BR}(M_{ij} \to l\nu) = G_F^2 m_l^2 f_M^2 \tau_M |V_{ij}|^2 \frac{m_M}{8\pi}\left(1 - \frac{m_l^2}{m_M^2}\right)^2 \left[|1 - \Delta_{ij}^{ll}|^2 + |\Delta_{ij}^{ll'}|^2\right], \tag{29}$$

where i, j are the valence quarks of the meson M, f_M is its decay constant and $\Delta_{ij}^{ll'}$ is the NP correction given by

$$\Delta_{ij}^{ll'} = \left(\frac{m_M}{m_{H^\pm}}\right)^2 Z_{ll'}\left(\frac{Y_{ij}m_{u_i} + X_{ij}m_{d_j}}{V_{ij}(m_{u_i} + m_{d_j})}\right), \qquad l, l' = 2, 3. \tag{30}$$

where the relations

$$X_{ij} = \frac{v}{\sqrt{2}m_{d_j}} V_{ik}\,\xi_{kj}^d, \qquad Y_{ij} = -\frac{v}{\sqrt{2}m_{u_i}} \xi_{ki}^{u*} V_{kj}, \qquad Z_{ij} = \frac{v}{\sqrt{2}m_j}\xi_{ij}^l, \tag{31}$$

depend on the Yukawa textures. The list of fully leptonic decays of mesons included in this analysis, for various mesons M, can be seen in Table 3.

Observable	Experiment
$\text{BR}(B_u \to \tau\nu) \times 10^4$	1.09 ± 0.24 [41]
$\frac{\text{BR}(K\to\mu\nu)}{\text{BR}(\pi\to\mu\nu)}$	0.6358 ± 0.0011 [42]
$\text{BR}(D_s \to \tau\nu) \times 10^2$	5.48 ± 0.23 [43]
$\text{BR}(D_s \to \mu\nu) \times 10^3$	5.49 ± 0.16 [43]
$\text{BR}(D \to \mu\nu) \times 10^4$	3.74 ± 0.17 [33]
$\text{BR}(D \to \tau\nu) \times 10^3$	1.20 ± 0.27 [44]

Table 3: *Additional leptonic decays of mesons considered in this work.*

4.4 Leptonic observables

There are a number of leptonic processes that are forbidden or suppressed in the SM but can occur in the GTHDM. These include modifications to the form factors for $\ell\ell'\gamma$, $\ell\ell'Z$ and other interactions, which lead to contributions to the anomalous magnetic moment of the muon, $(g-2)_\mu$, and LFV decays such as $\tau \to \mu\gamma$, $\tau \to 3\mu$ and $h \to \tau\mu$. In the SM, the contributions to these LFV observables are suppressed by the GIM mechanism, giving a very low experimental background, but in the GTHDM LFV is allowed at one- and two-loop level through the couplings ξ^l_{ij} in Eqs. (9-11). All of the experimental measurements and upper bounds for leptonic observables are shown in Table 4. For a more detailed explanation regarding the computation of the different contributions at the one and two loop level to Δa_μ in the GTHDM see [17].

Observable	Experiment
Δa_μ	$2.51 \pm 59 \times 10^{-9}$ [45]
BR($\tau \to \mu\gamma$)	$< 4.4 \times 10^{-8}$ at 90% C.L. [33]
BR($\tau \to 3\mu$)	$< 2.1 \times 10^{-8}$ at 95% C.L. [33]
BR($h \to \tau\mu$)	$< 1.5 \times 10^{-3}$ at 95% C.L. [46]
(g_μ/g_e)	1.0018 ± 0.0014 [47]

Table 4: *World average measurement of Δa_μ and experimental bounds for the LFV decay and LFU observables considered in our analysis.*

5. Results

We perform the global fit of all constraints using the inference package GAMBIT, the Global And Modular Beyond-the-Standard-Model Inference Tool[3]. GAMBIT is a powerful software framework capable of performing statistical inference studies using constraints from collider [51], dark matter [52], flavour [50] and neutrino [53] physics, as well as cosmology [54]. Our work enhances the FlavBit and PrecisionBit [55] modules of GAMBIT to support the GTHDM. We also make use of various external codes: SuperIso 4.1 [42, 56–58] for computing flavour observables, the 2HDMC 1.8 package [59] for precision electroweak constraints, the HEPLike package [60] which provides likelihoods for the neutral anomaly related observables, and the differential evolution sampler Diver 1.0.4 [61].

The theoretical predictions of the model and the experimental likelihoods are either implemented natively in GAMBIT or from external tools interfaced with GAMBIT. In particular, the likelihoods related to $b \to s\mu^+\mu^-$ transitions are obtained from HEPLike, which retrieves experimental results and their correlated uncertainties from the HEPLikeData repository. To efficiently explore the parameter space, we employ the differential evolution sampler Diver, which is a self-adaptive sampler. We choose a population size of NP = 20000 and a convergence threshold of convthresh = 10^{-6}. The data we present in this work comes from scans that took between 6 and 8

[3] GAMBIT is an open-source code and can be downloaded from its repository in https://github.com/GambitBSM/gambit_1.0 where all related manuals and documentation can be found, in particular the two main GAMBIT manuals can be found at [48, 49] and the FlavBit module manual is available at [50].

hours of running time on the Australian supercomputer GADI with cores varying between 1400 and 2000.

5.1 Parameter space

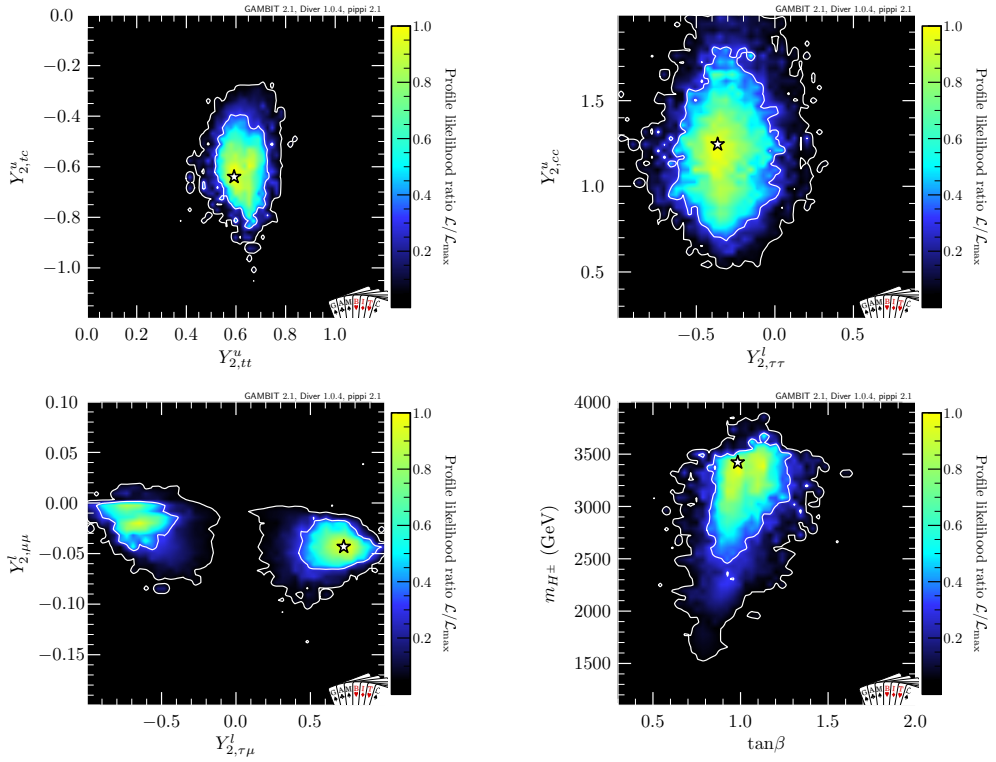

Figure 3: *Profile likelihood ratios $\mathcal{L}/\mathcal{L}_{max}$ for different 2D plots of the parameter space for $Y^u_{2,tc} \in [-2, 0]$.*

We perform the parameter scans in the physical basis, i.e., where the tree-level masses of the heavy Higgses, m_H, m_A and $m_{H^\pm}$ are taken as input. The remaining model parameters are $\tan\beta$, m_{12} and the Yukawa couplings $Y^f_{2,ij}$ as in Eq. (8). In order to avoid collider constraints, we work in the alignment limit choosing $s_{\beta-\alpha}$ close to 1, and we select a conservative lower limit on the masses of the heavy Higgses $m_{H,A,H^\pm} \geq 500$ GeV. We also fix $m_A = m_H$ in our study, motivated by the requirement to satisfy the oblique parameter constraints which favour small mass splittings and in order to simplify the sampling of the parameter space. The chosen priors on our scan parameters are

$$\begin{aligned}
&\tan\beta \in [0.2,\ 50], \qquad m_{12} \in [-1000,\ 2700]\,\text{GeV}, \qquad m_{H^\pm},\ m_A = m_H \in [500,\ 4000]\,\text{GeV},\\
&Y^u_{2,tt} \in [0.0,\ 2.0], \qquad Y^u_{2,cc},\ Y^u_{2,tc} \in [-2.0,\ 2.0],\\
&Y^d_{2,bb} \in [-0.1\,0.1], \qquad Y^d_{2,ss} \in [-0.2,\ 0.2], \qquad Y^d_{2,sb} = Y^d_{2,bs} \in [-0.01, 0.01],\\
&Y^l_{2,\mu\mu} \in [-0.5, 0.5], \qquad Y^l_{2,\tau\tau}\,, Y^l_{2,\mu\tau} = Y^l_{2,\tau\mu} \in [-1.0, 1.0],
\end{aligned} \tag{32}$$

We show in figure 3 different 2D planes with the most relevant parameters obtained by the scan. The values for $Y^u_{2,tt}$ and $Y^u_{2,tc}$ are displayed in the top left panel where we can observe that for the best

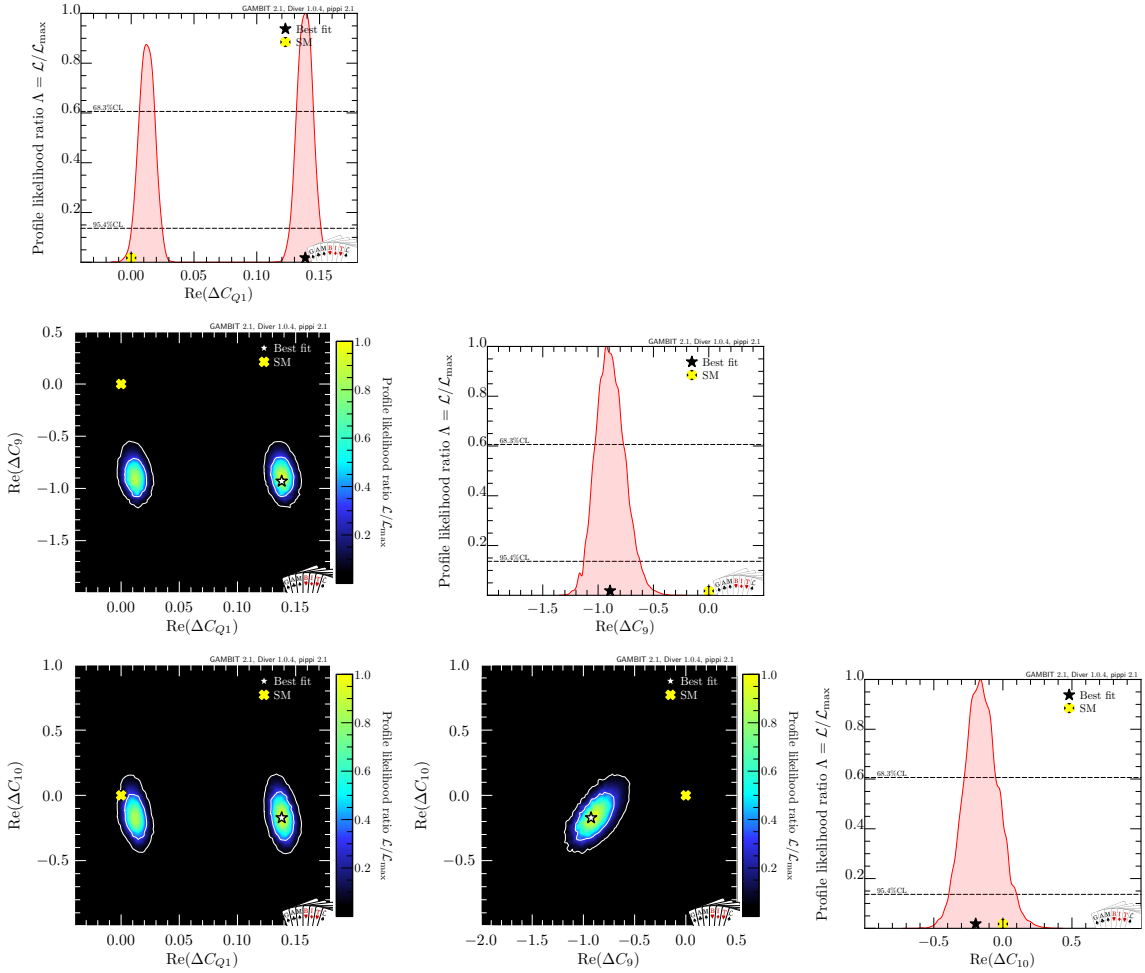

Figure 4: *One- and two-dimensional profile likelihoods for three of the Wilson coefficients computed from the fit.*

fit point $|Y^u_{2,tt}| \approx |Y^u_{2,tc}| \approx 0.6$. Then, in the top right panel we see a preferred value for $Y^u_{2,cc} \approx 1.1$ (-1.1 for the positive sign solution of $Y^u_{2,tc}$ from the degeneracy of solutions). This, along with the lepton Yukawa couplings $Y^l_{2,\mu\mu}$ and $Y^l_{2,\tau\mu}$ (bottom right panel), helps to enhance the contributions from the box diagrams in figures 2a-2b. Additionally, the LFV coupling $Y^l_{2,\tau\mu}$ also contributes to the $B^+ \to K^+\mu^\pm\tau^\mp$ decay, requiring $|Y^l_{2,\tau\mu}| \gtrsim 0.4$ in order to get $\mathrm{BR}(B^+ \to K^+\mu^\pm\tau^\mp) \times 10^5 < 4.8$. As for the $Y^d_{2,ij}$ couplings, we find $Y^d_{2,ss} = 0.1 \pm 0.1$, $Y^d_{2,sb} = 0.004 \pm 0.005$ and $Y^d_{2,bb} = 0.017 \pm 0.005$ assuming Gaussian distributions. In particular, both $Y^d_{2,ss}$ and $Y^d_{2,sb}$ flip their signs for the positive solutions of $Y^u_{2,tc}$ whereas $Y^d_{2,bb}$ remains unaffected.

Finally, in the bottom right panel of figure 3 we observe that the preferred values for the charged Higgs mass are of order 3 TeV with $\tan\beta \approx 1$. We find that the combined contribution of FCNC likelihoods fits better the data for this particular mass range. Similarly, although values of $\tan\beta$ up to 50 are possible in the GTHDM when using theoretical constraints alone, we identified that once we take into account all flavour constraints, there is a clear preference for low values, close to $\tan\beta \approx 1$, in agreement with [19, 62, 63].

5.2 Neutral and charged anomalies

We find values for the ΔC_9 WC consistent with model independent fits at the 1σ level. In this sense, the neutral anomalies can indeed be explained in the GTHDM as shown in figure 4. Furthermore, coming from the quadratic dependence in the branching ratio $\mathrm{BR}(B_s \to \mu^+\mu^-)$, we can see two regions of solutions for the scalar WC ΔC_{Q_1}, one of them containing the SM prediction within 2σ.

In order to better understand the contribution of the GTHDM to the various rates and angular observables, we display various plots comparing both the SM and the GTHDM predictions along the experimental data. We provide in figure 5 predictions for the angular observables in the S_i basis using the same LHCb 2020 measurements and also the ATLAS 2018 [64] data. We can see that the GTHDM fits better the LHCb data [65] in the large recoil region than the SM by 2σ. We also note that neither the SM or the GTHDM can explain the central values (with larger uncertainties) from the ATLAS 2018 data.

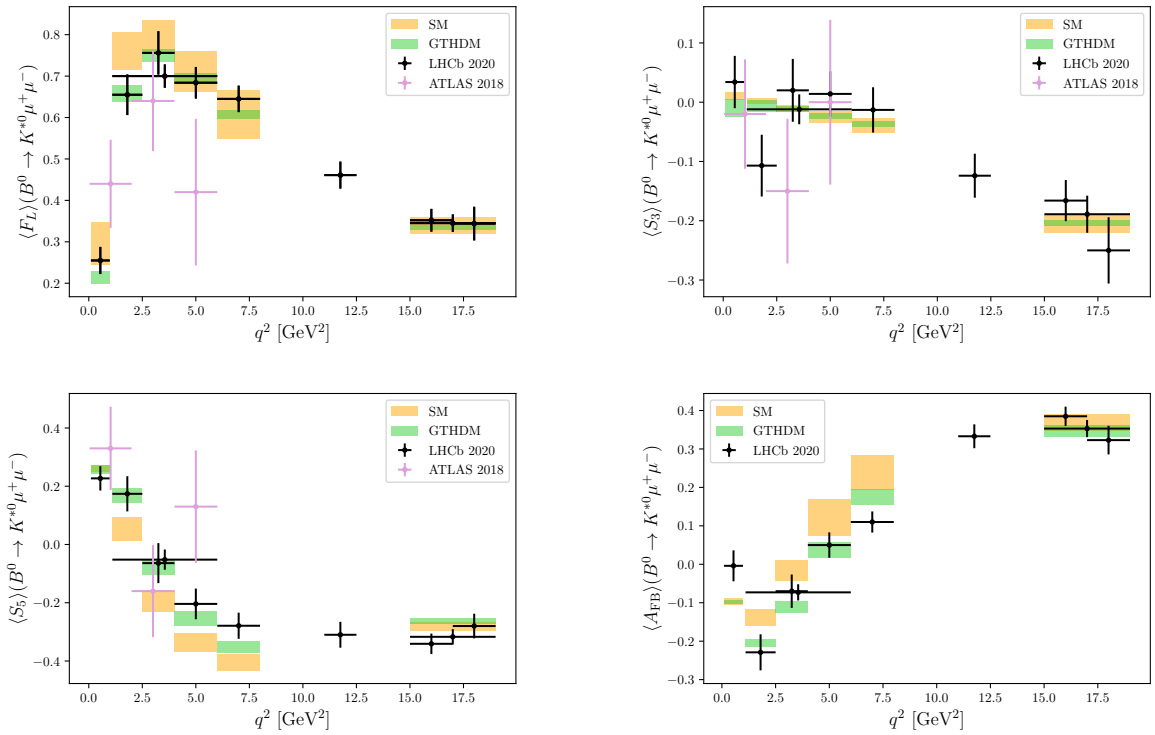

Figure 5: *Predicted distributions for the form factor dependent observables in the S_i basis using both the ATLAS 2018 [64] and the LHCb 2020 [65] data.*

Last but not least important observables related to the $b \to s\mu^+\mu^-$ transitions are the ratios $R(K^{(*)})$. Despite being only three bins in total [30, 31, 66], these measurements have been intensively studied as they provide evidence for LFU violation. We include in our fit the latest LHCb collaboration data for the $R(K^*)$ and $R(K)$ ratios from 2021 [31] and 2017 [30] respectively and obtain the plots in figure 6, where we compare also to the Belle 2019 experiment data [67, 68]. The effect from the fit on the $R(K^{(*)})$ ratios is significant, explaining the LHCb 2021 measurement

of $R(K)$ at the 1σ level.

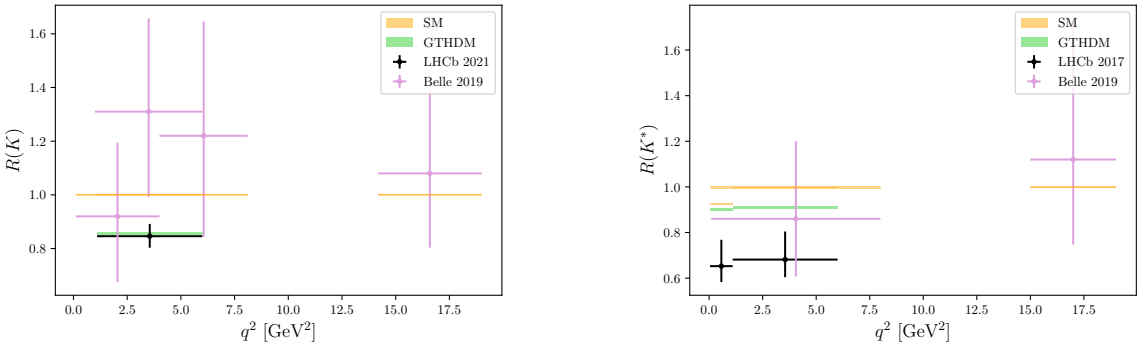

Figure 6: $R(K^{(*)})$ *theoretical ratios compared to both the LHCb [30, 31] and Belle data [67, 68].*

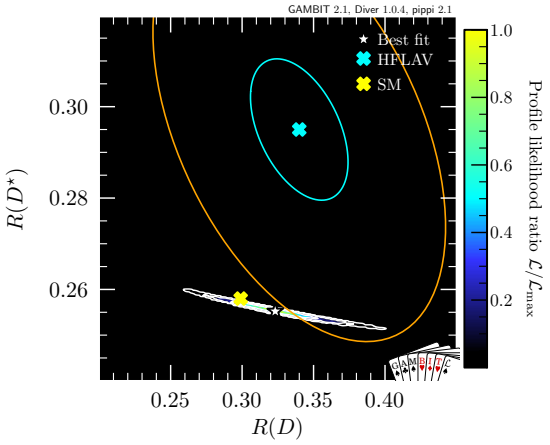

Figure 7: $R(D^*)$ *versus* $R(D)$ *correlated ratios. The cyan and orange lines are the* 1σ *and* 3σ *deviations from the HFLAV average respectively.*

The next interesting results are related with the charged anomalies, in particular we find that the $R(D^{(*)})$ ratio can (can not) be explained at the 1σ level with the GTHDM, a result in agreement with the phenomenological analysis of [40]. We furthermore corroborate that the constraint coming from the B_c lifetime makes it very difficult to fit $R(D^*)$ and $R(D)$ simultaneously. In figure 7 we show the preferred values by the profile likelihood. We see a slightly better performance of the GTHDM compared to the SM with respect to the HFLAV average. Regarding the $d\Gamma(B \to D^{(\star)}\tau\overline{\nu})/(\Gamma dq^2)$ distributions measured by BaBar [38], we find that the GTHDM prediction is indistinguishable from the SM, in agreement with [11]. We find furthermore that the longitudinal polarisation $F_L(D^*)$ is strongly correlated with $R(D^*)$ and the model is not able to explain the Belle measurement, giving a best fit value of 0.458 ± 0.006.

5.3 Anomalous $(g-2)_\mu$

With regards to the anomalous magnetic moment of the muon, $(g-2)_\mu$, we find that a simultaneous explanation using all the likelihoods defined before is not possible (solid red line in

figure 8). However, when doing a fit to all other observables except the neutral anomalies, i.e., without using the HEPLike likelihoods, the model is able to explain the measured Δa_μ by Fermilab at the 1σ level (dashed gray line in figure 8). Furthermore, when evaluating the performance of the HEPLike likelihoods for the best fit value, we find a SM-like behavior with all NP WCs close to zero, except for those scalar WCs that enter in $\mathrm{BR}(B_s \to \mu^+\mu^-)$.

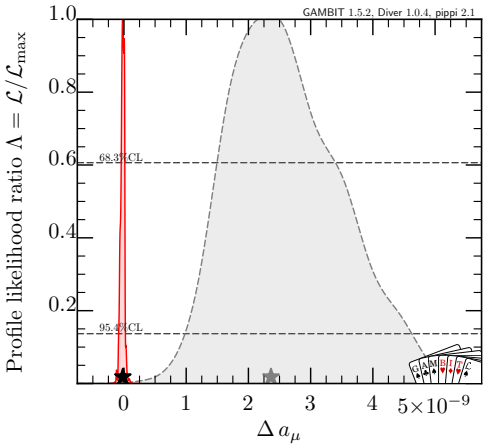

Figure 8: *One-dimensional profile likelihood for Δa_μ. The solid red line shows the result from the fit using all likelihoods and observables defined in this study. The dashed gray line is obtained using all but the HEPLike likelihoods instead.*

5.4 Projections for future and planned experiments

Regarding LFV searches, we show in figure 9 the profile likelihood for the $\tau \to 3\mu$ and $\tau \to \mu\gamma$ branching ratios. We see that the best fit value for the $\tau \to 3\mu$ decay is well within the projected sensitivity in the Belle II experiment [69] with a discovery potential for $\mathrm{BR}(\tau \to 3\mu) \sim 10^{-9}$. Regarding the $\tau \to \mu\gamma$ decay, we find that with the projected future sensitivity, the GTHDM prediction could be confirmed with values for the branching ratio varying from 10^{-9} up to 10^{-8}. As mentioned earlier, the $\tau \to 3\mu$ decay receives contributions in the GTHDM from all tree, dipole and contact terms, in such a way that a possible detection in the $\tau \to \mu\gamma$ channel will not necessarily imply a strong constraint for $\mathrm{BR}(\tau \to 3\mu)$.

Finally, with respect to $h \to \tau\mu$, with the model best fit point values, we computed the branching ratio $\mathrm{BR}(h \to \tau\mu)$ obtaining values from 10^{-2} down to 10^{-6} which are within the future sensitivity at the HL-LHC, reaching the 0.05% limit [70].

6. Conclusions and Outlook

We presented a frequentist inspired likelihood analysis for the GTHDM including the charged anomalies, $b \to s\mu^+\mu^-$ transitions and the anomalous magnetic moment of the muon along with other flavour observables. The analysis was carried out using the open source global fitting framework GAMBIT. We computed the GTHDM WCs and validated them obtaining full agreement with the one loop calculations reported in the literature. As expected, we found that the GTHDM

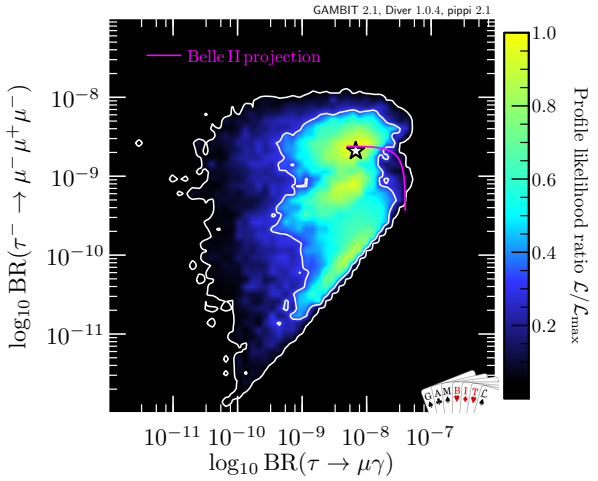

Figure 9: $\mathrm{BR}(\tau \to 3\mu)$ *versus* $\mathrm{BR}(\tau \to \mu\gamma)$. *The magenta solid line is the combined Belle II experiment future sensitivity obtained for both observables using a one-sided Gaussian upper limit likelihood function at 90%C.L.*

can explain the neutral anomalies at the 1σ level. Additionally, we also confirmed that the model is able to fit the current experimental values of the $R(D)$ ratio at the 1σ level, but it can not accommodate the D^* charmed meson observables $R(D^*)$ and $F_L(D^*)$. Furthermore, we inspected the fitted values for the angular observables in $b \to s\mu^+\mu^-$ transitions, obtaining in general a better performance with the GTHDM in comparison to the SM.

Then, based on the obtained best fit values of the model parameters and their 1σ and 2σ C.L. regions, we made predictions for $\mathrm{BR}(h \to \tau\mu)$ and the flavour violating decays of the τ lepton, $\mathrm{BR}(\tau \to 3\mu)$ and $\mathrm{BR}(\tau \to \mu\gamma)$. We find predictions for $\mathrm{BR}(h \to \tau\mu)$ that are within the future sensitivity of the HL-LHC or the ILC. Predictions for the $\tau \to 3\mu$ and $\tau \to \mu\gamma$ decays are alos well within the projected limits of the Belle II experiment.

Finally, in view of the latest experimental measurement made by the Fermilab Muon $g-2$ Collaboration, we performed a simultaneous fit to Δa_μ constrained by the charged anomalies finding solutions at the 1σ level. Once the neutral anomalies are included, however, a simultaneous explanation is unfeasible.

Acknowledgments

We would like to thank the organizers of the TOOLS 2021 conference for the opportunity to present our work. We also thank the Australian National Computational Infrastructure (NCI) for access to GADI. C.S was supported by the Monash Graduate Scholarship (MGS) and the Monash International Tuition Scholarship (MITS).

References

[1] S. P. Martin, *A Supersymmetry primer*, *Adv. Ser. Direct. High Energy Phys.* **18** (1998) 1–98, [hep-ph/9709356].

[2] R. D. Peccei and H. R. Quinn, *CP Conservation in the Presence of Instantons*, *Phys. Rev. Lett.* **38** (1977) 1440–1443.

[3] R. D. Peccei and H. R. Quinn, *Constraints Imposed by CP Conservation in the Presence of Instantons*, *Phys. Rev. D* **16** (1977) 1791–1797.

[4] D. Croon, T. E. Gonzalo, L. Graf, N. Košnik, and G. White, *GUT Physics in the era of the LHC*, *Front. in Phys.* **7** (2019) 76, [arXiv:1903.04977].

[5] **HFLAV**, Y. S. Amhis et al., *Averages of b-hadron, c-hadron, and τ-lepton properties as of 2018*, *Eur. Phys. J. C* **81** (2021), no. 3 226, [arXiv:1909.12524].

[6] M. Algueró, B. Capdevila, S. Descotes-Genon, J. Matias, and M. Novoa-Brunet, ***b → sℓℓ*** *global fits after Moriond 2021 results*, in *55th Rencontres de Moriond on QCD and High Energy Interactions*, 4, 2021. arXiv:2104.08921.

[7] T. Hurth, F. Mahmoudi, D. M. Santos, and S. Neshatpour, *More Indications for Lepton Nonuniversality in $b \to s\ell^+\ell^-$*, arXiv:2104.10058.

[8] J. Bhom, M. Chrzaszcz, F. Mahmoudi, M. Prim, P. Scott, and M. White, *A model-independent analysis of $b \to s\mu^+\mu^-$ transitions with GAMBIT's FlavBit*, arXiv:2006.03489.

[9] J. M. Cline, *Scalar doublet models confront τ and b anomalies*, *Phys. Rev. D* **93** (2016), no. 7 075017, [arXiv:1512.02210].

[10] S. Iguro and Y. Omura, *Status of the semileptonic B decays and muon g-2 in general 2HDMs with right-handed neutrinos*, *JHEP* **05** (2018) 173, [arXiv:1802.01732].

[11] R. Martinez, C. Sierra, and G. Valencia, *Beyond $\mathcal{R}(D^{(*)})$ with the general type-III 2HDM for $b \to c\tau\nu$*, *Phys. Rev. D* **98** (2018), no. 11 115012, [arXiv:1805.04098].

[12] J. Cardozo, J. H. Muñoz, N. Quintero, and E. Rojas, *Analysing the charged scalar boson contribution to the charged-current B meson anomalies*, *J. Phys. G* **48** (2021), no. 3 035001, [arXiv:2006.07751].

[13] P. Arnan, D. Bečirević, F. Mescia, and O. Sumensari, *Two Higgs doublet models and $b \to s$ exclusive decays*, *Eur. Phys. J. C* **77** (2017), no. 11 796, [arXiv:1703.03426].

[14] A. Arhrib, R. Benbrik, C. H. Chen, J. K. Parry, L. Rahili, S. Semlali, and Q. S. Yan, *$R_{K^{(*)}}$ anomaly in type-III 2HDM*, arXiv:1710.05898.

[15] A. Crivellin, D. Muller, and C. Wiegand, *$b \to s\ell^+\ell^-$ transitions in two-Higgs-doublet models*, *JHEP* **06** (2019) 119, [arXiv:1903.10440].

[16] J. Herrero-Garcia, M. Nebot, F. Rajec, M. White, and A. G. Williams, *Higgs Quark Flavor Violation: Simplified Models and Status of General Two-Higgs-Doublet Model*, *JHEP* **02** (2020) 147, [arXiv:1907.05900].

[17] P. Athron, C. Balazs, T. E. Gonzalo, D. Jacob, F. Mahmoudi, and C. Sierra, *Likelihood analysis of the flavour anomalies and g – 2 in the general two Higgs doublet model*, *JHEP* **01** (2022) 037, [arXiv:2111.10464].

[18] S. Davidson and H. E. Haber, *Basis-independent methods for the two-Higgs-doublet model*, *Phys. Rev. D* **72** (2005) 035004, [hep-ph/0504050]. [Erratum: Phys.Rev.D 72, 099902 (2005)].

[19] G. Branco, P. Ferreira, L. Lavoura, M. Rebelo, M. Sher, and J. P. Silva, *Theory and phenomenology of two-Higgs-doublet models*, *Phys. Rept.* **516** (2012) 1–102, [arXiv:1106.0034].

[20] H. E. Haber and D. O'Neil, *Basis-independent methods for the two-Higgs-doublet model III: The CP-conserving limit, custodial symmetry, and the oblique parameters S, T, U*, *Phys. Rev. D* **83** (2011) 055017, [arXiv:1011.6188].

[21] J. Hernandez-Sanchez, S. Moretti, R. Noriega-Papaqui, and A. Rosado, *Off-diagonal terms in Yukawa textures of the Type-III 2-Higgs doublet model and light charged Higgs boson phenomenology*, *JHEP* **07** (2013) 044, [arXiv:1212.6818].

[22] A. Crivellin, C. Greub, and A. Kokulu, *Flavor-phenomenology of two-Higgs-doublet models with generic Yukawa structure*, *Phys. Rev. D* **87** (may, 2013) 094031.

[23] C. Degrande, *Automatic evaluation of UV and R2 terms for beyond the Standard Model Lagrangians: a proof-of-principle*, *Comput. Phys. Commun.* **197** (2015) 239–262, [arXiv:1406.3030].

[24] V. Shtabovenko, R. Mertig, and F. Orellana, *New Developments in FeynCalc 9.0*, *Comput. Phys. Commun.* **207** (2016) 432–444, [arXiv:1601.01167].

[25] H. H. Patel, *Package-X: A Mathematica package for the analytic calculation of one-loop integrals*, *Comput. Phys. Commun.* **197** (2015) 276–290, [arXiv:1503.01469].

[26] G. Uhlrich, F. Mahmoudi, and A. Arbey, *MARTY - Modern ARtificial Theoretical phYsicist A C++ framework automating symbolic calculations Beyond the Standard Model*, *Comput. Phys. Commun.* **264** (2021) 107928, [arXiv:2011.02478].

[27] A. Celis, M. Jung, X.-Q. Li, and A. Pich, *Sensitivity to charged scalars in $B \to D^{(*)}\tau\nu_\tau$ and $B \to \tau\nu_\tau$ decays*, *JHEP* **01** (2013) 054, [arXiv:1210.8443].

[28] A. Crivellin, C. Greub, and A. Kokulu, *Explaining $B \to D\tau\nu$, $B \to D^*\tau\nu$ and $B \to \tau\nu$ in a 2HDM of type III*, *Phys. Rev. D* **86** (2012) 054014, [arXiv:1206.2634].

[29] R. Alonso, B. Grinstein, and J. Martin Camalich, *Lifetime of B_c^- Constrains Explanations for Anomalies in $B \to D^{(*)}\tau\nu$*, *Phys. Rev. Lett.* **118** (2017), no. 8 081802, [arXiv:1611.06676].

[30] **LHCb**, R. Aaij et al., *Test of lepton universality with $B^0 \to K^{*0}\ell^+\ell^-$ decays*, *JHEP* **08** (2017) 055, [arXiv:1705.05802].

[31] **LHCb**, R. Aaij et al., *Test of lepton universality in beauty-quark decays*, arXiv:2103.11769.

[32] **LHCb Collaboration**, *Combination of the ATLAS, CMS and LHCb results on the $B^0_{(s)} \to \mu^+\mu^-$ decays*, tech. rep., CERN, Geneva, Aug, 2020.

[33] **Particle Data Group**, P. A. Zyla et al., *Review of Particle Physics*, *PTEP* **2020** (2020), no. 8 083C01.

[34] **Belle**, J. Grygier et al., *Search for $B \to h\nu\bar{\nu}$ decays with semileptonic tagging at Belle*, *Phys. Rev. D* **96** (2017), no. 9 091101, [arXiv:1702.03224]. [Addendum: Phys.Rev.D 97, 099902 (2018)].

[35] J. Bhom and M. Chrząszcz, *HEPLikeData*, 2020. https://github.com/mchrzasz/HEPLikeData.

[36] **Belle**, E. Waheed et al., *Measurement of the CKM matrix element $|V_{cb}|$ from $B^0 \to D^{*-}\ell^+\nu_\ell$ at Belle*, *Phys. Rev. D* **100** (2019), no. 5 052007, [arXiv:1809.03290]. [Erratum: Phys.Rev.D 103, 079901 (2021)].

[37] **Belle**, A. Abdesselam et al., *Measurement of the D^{*-} polarization in the decay $B^0 \to D^{*-}\tau^+\nu_\tau$*, in *10th International Workshop on the CKM Unitarity Triangle*, 3, 2019. arXiv:1903.03102.

[38] **BaBar**, J. Lees et al., *Measurement of an Excess of $\bar{B} \to D^{(*)}\tau^-\bar{\nu}_\tau$ Decays and Implications for Charged Higgs Bosons*, *Phys. Rev. D* **88** (2013), no. 7 072012, [arXiv:1303.0571].

[39] M. Jung, A. Pich, and P. Tuzon, *Charged-Higgs phenomenology in the Aligned two-Higgs-doublet model*, *JHEP* **11** (2010) 003, [arXiv:1006.0470].

[40] S. Iguro and K. Tobe, *$R(D^{(*)})$ in a general two Higgs doublet model*, *Nucl. Phys. B* **925** (2017) 560–606, [arXiv:1708.06176].

[41] **Heavy Flavor Averaging Group**, E. Barberio et al., *Averages of b−hadron and c−hadron Properties at the End of 2007*, arXiv:0808.1297.

[42] F. Mahmoudi, *SuperIso v2.3: A Program for calculating flavor physics observables in Supersymmetry*, *Comput. Phys. Commun.* **180** (2009) 1579–1613, [arXiv:0808.3144].

[43] A. G. Akeroyd and F. Mahmoudi, *Constraints on charged Higgs bosons from $D_s^\pm \to \mu^\pm\nu$ and $D_s^\pm \to \tau^\pm\nu$*, *JHEP* **04** (2009) 121, [arXiv:0902.2393].

[44] **Particle Data Group**, P. A. Zyla et al., *Review of Particle Physics*, *PTEP* **2020** (2020), no. 8 083C01.

[45] **Muon $g-2$ Collaboration**, B. Abi et al., *Measurement of the positive muon anomalous magnetic moment to 0.46 ppm*, *Phys. Rev. Lett.* **126** (Apr, 2021) 141801.

[46] **CMS**, A. M. Sirunyan et al., *Search for lepton-flavor violating decays of the Higgs boson in the $\mu\tau$ and $e\tau$ final states in proton-proton collisions at $\sqrt{s} = 13$ TeV*, arXiv:2105.03007.

[47] S. Bifani, S. Descotes-Genon, A. Romero Vidal, and M.-H. Schune, *Review of Lepton Universality tests in B decays*, *J. Phys. G* **46** (2019), no. 2 023001, [arXiv:1809.06229].

[48] **GAMBIT Collaboration**, P. Athron et al., *GAMBIT: The Global and Modular Beyond-the-Standard-Model Inference Tool*, *Eur. Phys. J. C* **77** (2017), no. 11 784, [arXiv:1705.07908]. [Addendum: Eur.Phys.J.C 78, 98 (2018)].

[49] A. Kvellestad, P. Scott, and M. White, *GAMBIT and its Application in the Search for Physics Beyond the Standard Model*, *Prog. Part. Nuc. Phys.* **113** (2020) 103769, [arXiv:1912.04079].

[50] **GAMBIT Flavour Workgroup**, F. U. Bernlochner et al., *FlavBit: A GAMBIT module for computing flavour observables and likelihoods*, *Eur. Phys. J. C* **77** (2017), no. 11 786, [arXiv:1705.07933].

[51] **GAMBIT Collider Workgroup**, C. Balázs et al., *ColliderBit: a GAMBIT module for the calculation of high-energy collider observables and likelihoods*, *Eur. Phys. J. C* **77** (May, 2017) 795, [arXiv:1705.07919].

[52] **GAMBIT Dark Matter Workgroup**, T. Bringmann et al., *DarkBit: A GAMBIT module for computing dark matter observables and likelihoods*, *Eur. Phys. J. C* **77** (May, 2017) 831, [arXiv:1705.07920].

[53] M. Chrzaszcz, M. Drewes, T. E. Gonzalo, J. Harz, S. Krishnamurthy, and C. Weniger, *A frequentist analysis of three right-handed neutrinos with GAMBIT*, *Eur. Phys. J. C* **80** (2020), no. 6 569, [arXiv:1908.02302].

[54] **GAMBIT Cosmology Workgroup**, J. J. Renk et al., *CosmoBit: A GAMBIT module for computing cosmological observables and likelihoods*, *JCAP* **02** (2021) 022, [arXiv:2009.03286].

[55] **GAMBIT Models Workgroup**, P. Athron et al., *SpecBit, DecayBit and PrecisionBit: GAMBIT modules for computing mass spectra, particle decay rates and precision observables*, *Eur. Phys. J. C* **78** (2018), no. 1 22, [arXiv:1705.07936].

[56] F. Mahmoudi, *SuperIso: A Program for calculating the isospin asymmetry of B —> K* gamma in the MSSM*, *Comput. Phys. Commun.* **178** (2008) 745–754, [arXiv:0710.2067].

[57] F. Mahmoudi, *SuperIso v3.0, flavor physics observables calculations: Extension to NMSSM*, *Comput. Phys. Commun.* **180** (2009) 1718–1719.

[58] S. Neshatpour and F. Mahmoudi, *Flavour Physics with SuperIso*, *PoS* **TOOLS2020** (2021) 036, [arXiv:2105.03428].

[59] D. Eriksson, J. Rathsman, and O. Stal, *2HDMC: Two-Higgs-Doublet Model Calculator Physics and Manual*, *Comput. Phys. Commun.* **181** (2010) 189–205, [arXiv:0902.0851].

[60] J. Bhom and M. Chrzaszcz, *HEPLike: an open source framework for experimental likelihood evaluation*, *Comput. Phys. Commun.* **254** (2020) 107235, [arXiv:2003.03956].

[61] **GAMBIT Collaboration**, G. D. Martinez, J. McKay, B. Farmer, P. Scott, E. Roebber, A. Putze, and J. Conrad, *Comparison of statistical sampling methods with ScannerBit, the GAMBIT scanning module*, *Eur. Phys. J. C* **77** (2017), no. 11 761, [arXiv:1705.07959].

[62] A. Wahab El Kaffas, P. Osland, and O. M. Ogreid, *Constraining the Two-Higgs-Doublet-Model parameter space*, *Phys. Rev. D* **76** (2007) 095001, [arXiv:0706.2997].

[63] A. Arhrib, R. Benbrik, C.-H. Chen, R. Guedes, and R. Santos, *Double Neutral Higgs production in the Two-Higgs doublet model at the LHC*, *JHEP* **08** (2009) 035, [arXiv:0906.0387].

[64] **ATLAS**, M. Aaboud et al., *Angular analysis of* $B^0_d \to K^*\mu^+\mu^-$ *decays in* pp *collisions at* $\sqrt{s} = 8$ *TeV with the ATLAS detector*, *JHEP* **10** (2018) 047, [arXiv:1805.04000].

[65] **LHCb**, R. Aaij et al., *Measurement of CP-Averaged Observables in the* $B^0 \to K^{*0}\mu^+\mu^-$ *Decay*, *Phys. Rev. Lett.* **125** (2020), no. 1 011802, [arXiv:2003.04831].

[66] **LHCb**, R. Aaij et al., *Search for lepton-universality violation in* $B^+ \to K^+\ell^+\ell^-$ *decays*, *Phys. Rev. Lett.* **122** (2019), no. 19 191801, [arXiv:1903.09252].

[67] **Belle**, A. Abdesselam et al., *Test of Lepton-Flavor Universality in* $B \to K^*\ell^+\ell^-$ *Decays at Belle*, *Phys. Rev. Lett.* **126** (2021), no. 16 161801, [arXiv:1904.02440].

[68] **BELLE**, S. Choudhury et al., *Test of lepton flavor universality and search for lepton flavor violation in* $B \to K\ell\ell$ *decays*, *JHEP* **03** (2021) 105, [arXiv:1908.01848].

[69] **Belle-II**, W. Altmannshofer et al., *The Belle II Physics Book*, *PTEP* **2019** (2019), no. 12 123C01, [arXiv:1808.10567]. [Erratum: PTEP 2020, 029201 (2020)].

[70] W.-S. Hou and G. Kumar, *Coming decade of* $h \to \tau\mu$ *and* $\tau \to \mu\gamma$ *interplay in* τ *flavor violation search*, *Phys. Rev. D* **101** (2020), no. 9 095017, [arXiv:2003.03827].